

RSC Advances



This is an *Accepted Manuscript*, which has been through the Royal Society of Chemistry peer review process and has been accepted for publication.

Accepted Manuscripts are published online shortly after acceptance, before technical editing, formatting and proof reading. Using this free service, authors can make their results available to the community, in citable form, before we publish the edited article. This *Accepted Manuscript* will be replaced by the edited, formatted and paginated article as soon as this is available.

You can find more information about *Accepted Manuscripts* in the [Information for Authors](#).

Please note that technical editing may introduce minor changes to the text and/or graphics, which may alter content. The journal's standard [Terms & Conditions](#) and the [Ethical guidelines](#) still apply. In no event shall the Royal Society of Chemistry be held responsible for any errors or omissions in this *Accepted Manuscript* or any consequences arising from the use of any information it contains.

**Influence of Oxodiperoxovanadate Complexes on Prion
Neuropeptide Fibril Formation**

Baohong Zhang,^{1,2} Dengsen Zhu,¹ Wenji Wang,¹ Gehui Gong,¹ Weihong Du^{1,*}

¹*Department of Chemistry, Renmin University of China, Beijing, 100872, China*

²*College of Materials Science and Engineering, North University of China,
Taiyuan, 030051, China*

Abstract

The neuropeptide PrP106-126 is used as a common model to study abnormal prion proteins. Some metal complexes are able to inhibit the formation of PrP106-126 fibrils and various compounds exhibit diverse interaction mechanisms. In this study, four oxodiperoxovanadate complexes were examined for inhibition of fibril formation of PrP106-126 and the mutant peptide M109F. Compounds **1**, **3**, and **4** directly interacted with the peptide or induced methionine oxidation. However, complex **2**, which contains a large aromatic ligand, eliminated methionine oxidation activity and altered the inhibitory mechanism via steric effects. Aggregation was assessed by thioflavine T fluorescence and morphology analyses and complexes **1**, **3**, and **4** significantly decreased peptide fibril formation in comparison to **2**. However, **2** caused increased cellular viability against amyloid peptide-induced cytotoxicity. This work elucidated the distinct role of a large aromatic ligand in peptide aggregation, binding affinity, and cytotoxicity.

Keywords: PrP106-126, fibril formation, methionine oxidation, oxodiperoxovanadium complexes, ligand steric effect.

*Corresponding Author. E-mail for W. Du: whdu@chem.ruc.edu.cn

Introduction

Metal complexes are potential therapeutic agents against various diseases. Platinum, gold, and ruthenium compounds are widely used as anticancer agents.¹⁻³ These compounds may also inhibit fibril formation of amyloid proteins, including A β protein, human islet amyloid polypeptide (hIAPP), and prion neuropeptide.⁴⁻⁹ This inhibition may be attributed to metal coordination, as well as hydrophobic and electrostatic interactions. Therefore, development of metal complexes with decreased cytotoxicity and enhanced inhibitory efficacy has potential applications for use as therapies against amyloid-related diseases. Vanadium compounds are insulin mimetic agents for the treatment of type I and type II diabetes.¹⁰⁻¹³ Vanadium has been applied since the 19th century to decrease glucose levels, and new vanadium compounds are continuously being synthesized.^{14,15} In addition, these compounds can also be used to treat endemic diseases, such as dengue fever and SARS,¹⁶⁻¹⁸ and these complexes exhibit anticancer activities due to their interactions with DNA. However, clinical antitumor applications of vanadium complexes are limited. Several studies have documented that peroxovanadium species mimic insulin via phosphotyrosine phosphatase inhibition, and prevent cancerous tumor growth by inducing DNA cleavage.^{19,20} Peroxovanadium species were recently investigated for their ability to inhibit the fibril formation of hIAPP, which is correlated with type II diabetes. Vanadium complexes with aromatic ligands led to increased inhibition against hIAPP aggregation, suggesting a putative and distinct role in the treatment of diabetes.¹³ Another study discovered that peroxovanadate complexes inhibit the aggregation of

both A β protein and a prion neuropeptide (PrP106-126) by methionine oxidation.²¹ However, the role of ligands and the redox property of vanadate were not completely characterized.

Prion disease is a neurodegenerative disease found in a variety of animal species, including humans. Several neurological diseases in humans have been identified and are currently regarded as prion diseases, including Creutzfeldt-Jakob disease, Kuru, fatal familial insomnia, and Gerstmann-Sträussler-Scheinker syndrome.²² Since Creutzfeldt-Jakob disease was first reported in 1996, there have been a total of 229 confirmed cases worldwide, with a majority of cases occurring in the UK. Among the 4 cases confirmed in the US, 3 of the individuals had a history of residing in the UK.²³ Prion diseases are invariably fatal neurodegenerative disorders, annually affecting ~1 person per million inhabitants worldwide.²⁴ A recent study indicated that a naturally occurring variant of human prion protein (PrP) may completely prevent the prion disease.²⁵ The pathogenesis of prion disease is related to conformational changes in the normal prion protein (PrP^C) to cause amyloid fibril formation of the abnormal prion protein (PrP^{Sc}).^{26,27} PrP^{Sc} is considered to be an infectious agent due to several biological properties that are profoundly different from those of native PrP^C.²⁸ PrP^{Sc} has more β sheets and fewer α helix structures than PrP^C. Accumulation of PrP^{Sc} in the central nervous system of affected individuals leads to nerve cell dysfunction.²⁹ PrP106-126, an N-terminal fragment of PrP, is an important prion neuropeptide. This peptide exhibits analogous properties to PrP^{Sc} in many aspects, including

fibrillogenesis, cellular toxicity, and membrane-binding affinity.³⁰⁻³⁶ Thus, this peptide is commonly used as a model for studying PrP^{Sc}.

Various inhibitors against amyloidogenic proteins have been studied in recent years. Metal ions, short peptides, and aromatic compounds have been utilized to inhibit and reverse conformational changes of the pathological protein, which also inhibits sequential fibril formation.^{37,38} Ruthenium and gold compounds were employed to eliminate misfolded aggregates of PrP106-126 and its mutants in previous studies.³⁹⁻⁴² These compounds exhibit enhanced inhibitory effects against amyloid fibril formation and repress the cytotoxicity induced by PrP106-126. Gold complexes possess strong binding affinities with the peptide, and a gold ion is bound by residues His111 and Met102 via metal coordination. NAMI-A-like ruthenium complexes interact with PrP106-126 mainly via electrostatic interactions.⁴¹ The contributions of the molecular structure and properties were characterized from these complexes. In the present study, four oxodiperoxovanadate complexes with different molecular structures and ligands (Scheme 1) were utilized to probe their interactions with PrP106-126 and the M109F mutant peptide in order to examine the factors that influence fibril formation and explore the interacting mechanisms of vanadium complexes with PrP106-126. These complexes are: $(\text{NH}_4)_3[\text{VO}(\text{O}_2)_2(\text{ox})]\cdot 2\text{H}_2\text{O}$ (**1**), $(\text{H}_2\text{bipy})[\text{V}_2\text{O}_2(\text{O}_2)_4(\text{bipy})_2]\cdot 6\text{H}_2\text{O}$ (**2**), $\text{Na}[\text{VO}(\text{O}_2)_2]\cdot \text{Na}_2\text{SO}_4$ (**3**), and $\text{K}_2[\text{nicH}\{\text{VO}(\text{O}_2)_2\}_2]\cdot \text{H}_2\text{O}$ (**4**) (ox represents oxalic acid, bipy symbolizes 2,2-dipyridyl and nicH stands for nicotinic acid). The complexes containing coordinated and protonated nitrogen ligands can be formulated as $(\text{LH}_2)\text{H}_2[\text{O}\{\text{VO}(\text{O}_2)_2(\text{bipy})\}_2]\cdot 5\text{H}_2\text{O}$ in view of

the structure found in dimeric peroxovanadate complexes, compatible with the spectral data.⁴³⁻⁴⁵ Therefore, complex **2** may be represented by its $5\text{H}_2\text{O}$ formulae (see Scheme 1 and supporting Fig. S1). The complexes were selected based on their potential redox capabilities and differences in ligand aromaticity. The results indicated that the complexes inhibited the fibril formation of PrP106-126 and the M109F peptide through direct binding and site-specific methionine oxidation. However, the four compounds exhibited different efficacies, which were attributed to their distinct molecular structures and inhibitory mechanisms.

Experimental protocols

Materials

Human prion neuropeptide PrP106-126 (106-KTNMKHMAGAAAAGAVVGG-LG-126) and its mutant M109F were chemically synthesized and purified by SBS Co., Ltd. (Beijing, China). The final products with >95% purity were identified through High performance liquid chromatography (HPLC) and mass spectroscopy (MS). The oxodiperoxovanadate complexes were prepared and identified by ^1H NMR and IR spectra based on previously reported studies.^{44,46,47} All other reagents were of analytical grade.

Thioflavine T (ThT) assay

The ThT fluorescence was excited at 432 nm, and the emission fluorescence at approximately 500 nm was determined using the average value from 3 experiments. The excitation and emission slit was 10 nm, the scan speed was 240 nm min⁻¹, and the PMT voltage was 700 V. A 100 μM solution of PrP106-126 or its mutant M109F in 10 mM phosphate buffer (pH 7.4) was incubated at 310 K for 24 h. The oxodiperoxovanadate complex was then added and incubated for additional 24 h. After incubation, 100 μM ThT was added, and fluorescence monitored by F-4600 spectrofluorometer (Hitachi Ltd., Japan).

Morphology

The transmission electron microscope (TEM) sample was prepared using a 100 μM solution of PrP106-126 or its mutant M109F, and incubated at 310 K for 24 h. Two equivalents or 10 equivalents of the oxodiperoxovanadate complexes were added and incubated for 24 h. An aliquot of each sample was spotted onto carbon-coated 600-mesh copper grids and negatively stained with 2% phosphotungstic acid. The final peptide concentration used in the TEM experiment was 10 μM. The air-dried specimens were examined and photographed using Hitachi H-800 electron microscope (Hitachi, Japan) at 200 kV. The final image used was the mean of the 3 repeated data. For atomic force microscope (AFM) analysis, 100 μM solution of PrP106-126 or its mutant M109F was incubated at 310 K for 24 h. Two equivalents of oxodiperoxovanadate complexes were then added and incubated for additional 24 h.

The final peptide concentration in the AFM experiment was 10 μM . Images were obtained using the Veeco D3100 apparatus (Veeco Instruments 151, Inc., USA) in the tapping mode with a silicon tip under ambient conditions at a scanning rate of 1 Hz and a scanning line of 512.

Electrospray Ionization-Mass spectroscopy (ESI-MS)

To obtain the ESI-MS spectra, we introduced the samples directly at a flow rate of 3 $\mu\text{L min}^{-1}$. The spectra were recorded in a positive mode on an APEX IVFT-ICR high-resolution mass spectrometer (Bruker, USA) equipped with a conventional ESI source. The following conditions were applied: end-plate electrode voltage of -3500 V, capillary entrance voltage of -4000 V, skimmers of 1 and 30 V, dry gas temperature of 473 K, drying gas flow rate of 12 L min^{-1} , and nebulizer gas flow rate of 6 L min^{-1} . Data were acquired using the Data Analysis 4.0 software (Bruker). Deconvoluted masses were obtained using an integrated deconvolution tool. The peptide samples were maintained at 50 μM in the ESI-MS experiment. Two equivalents of oxodiperoxovanadate complexes were added to the peptide samples to validate the assay. All samples were incubated for 12 h before use.

NMR spectra

The ^1H NMR spectrum of PrP106-126 or its mutant peptide M109F was recorded at a pH value of 5.7 and a temperature of 298 K using a Bruker Avance 400/600 MHz NMR spectrometer. Two equivalents of the oxodiperoxovanadate complexes were added in the peptide solution, and spectra were obtained continuously for 3 h. The final peptide concentration was 0.5 mM. A watergate pulse program with gradients was applied to suppress the residual water signal.

Intrinsic fluorescence method

Steady-state fluorescence measurements of the intrinsic phenylalanine residue were conducted at room temperature to detect the binding ability of oxodiperoxovanadate complexes to peptide M109F. The excitation wavelength of 260 nm was chosen in accordance with previous studies.^{48,49} The dissociation constant (K_d) was determined from the fluorescence intensity plot via oxodiperoxovanadate complex concentration using eqn (1):

$$\Delta F = F_0 - F_L = (F_0 - F_a) \left\{ K_d + P_0 + T - [(K_d + P_0 + T)^2 - 4P_0T]^{1/2} \right\} / 2P_0 \quad (1)$$

where F_0 and F_L are the measured peptide fluorescence intensities at 287 nm in the absence and presence of oxodiperoxovanadate complexes, respectively; F_a is the maximum quenching of the peptide fluorescence; P_0 refers to the initial concentration of the peptide; T represents the concentration of the added oxodiperoxovanadate complex. The solution was prepared in 10 mM phosphate buffer at pH 7.4. The

concentration of the peptide M109F was 100 μM . The results were obtained from 3 repeated experiments.

HPLC

A 100 μM solution of PrP106-126 or its mutant peptide M109F in 10 mM phosphate buffer (pH 7.4) was incubated at 310 K for 24 h. Two equivalents of oxodiperoxovanadate complexes were then added, and the mixture was incubated for the next 24 h. After incubation, the samples were centrifuged, loaded, and eluted with a gradient beginning with solvent A (0.1% trifluoroacetic acid) and solvent B (0.1% trifluoroacetic acid/acetonitrile), and analyzed by reverse HPLC with a Calesil ODS-100 C18 column (4.6 mm \times 250 mm). A linear gradient was used as follows: 0–1 min, 5%–10% B; 1–25 min, 10%–50% B; 25–28 min, 50%–95% B, at a flow rate of 1 mL min^{-1} .

MTT assay

Human SH-SY5Y neuroblastoma cells were cultured in a 1:1 mixture of Dulbecco's Modified Eagle's Medium and F12 medium supplemented with 10% fetal bovine serum, 2 mM glutamine, 100 U mL^{-1} penicillin, and 100 U mL^{-1} streptomycin. The cells were maintained at 310 K in a humidified incubator in 95% air and 5% CO_2 . Cell survival was assessed by measuring the reduction of 3-(4,5-dimethyl-

2-thiazolyl)-2,5-diphenyl-2-H-tetrazolium bromide (MTT). A 100 μM PrP106-126 solution was incubated for 24 h with or without 1, 10, or 50 μM oxodiperoxovanadate complex, and the mixture was added to the cells. After reaction for 4 d, the cells were incubated with 10 μL of MTT at 310 K for 4 h. The absorbance at 570 nm was recorded using a Cary 50 UV-vis spectrophotometer (Varian, Inc., USA). Each experiment was conducted in quadruplicates. Data were calculated as percentage of the untreated control value.

Results

Peptide aggregation

Four oxodiperoxovanadate complexes were synthesized and identified as previously described methods^{44,46,47} and the effect of these complexes on the aggregation of PrP106-126 and mutant peptide M109F was evaluated. ThT is a dye that fluoresces when it binds to aggregated amyloid peptides and therefore represents the extent of amyloid peptide aggregation. Incubation of the vanadium complexes with the peptide resulted in a marked decrease in ThT fluorescence intensity. The vanadium complexes exhibited no interactions with ThT, as previously reported.²¹ Thus, the reduction was attributed to metal complexes binding to or reacting with the aggregated peptide (Fig. 1). Moreover, the influence of vanadium complexes on prion peptide aggregation was concentration-dependent (supporting Fig. S2). The IC_{50} values of the compounds on peptide aggregation (Table 1) were determined using a previously reported method.^{50,51} Data from the ThT assay indicated that complex **3** effectively inhibited

peptide aggregation; the IC_{50} values for complex **3** with PrP106-126 and peptide M109F were $14.88 \pm 0.13 \mu\text{M}$ and $10.65 \pm 1.35 \mu\text{M}$, respectively. In contrast, complex **2** exhibited relatively high IC_{50} values of $77.50 \pm 2.50 \mu\text{M}$ and $89.75 \pm 0.26 \mu\text{M}$ for PrP106-126 and peptide M109F, respectively. In addition, the vanadium complexes appeared to compete with ThT for peptide binding (Fig. S3), which necessitated additional further experiments in order to clarify the influence of the vanadium compounds on peptide fibril formation.

TEM and AFM images

The morphology of peptide fibrils was assessed using TEM and AFM images. Self-assembly of PrP106-126 produced a distinct fibril structure after a 24 h incubation at 310 K (Fig. 2). In contrast, the mutant peptide M109F had fewer fibrils than PrP106-126, indicating that Met109 is important for aggregation (Fig. S4). The presence of two equivalents of vanadium complexes effectively inhibited peptide aggregation, which led to fewer fibrils and spherical aggregates. When the molar ratio of metal complex:peptide was 1:10, the complex further inhibited peptide aggregation of PrP106-126. Interestingly, the compounds caused less inhibition of aggregation for peptide M109F in comparison to PrP106-126 (Figs. 3 & S5). The TEM results for complex **2** were similar to the ThT assay, indicating that **2** had a weaker influence on aggregation relative to other compounds. AFM images were collected at two equivalents of complex **2** in order to clarify TEM results (Figs. 4 & S6). The data indicated that complex **3** had enhanced inhibition of peptide aggregation for both

PrP106-126 and peptide M109F and these results are consistent with those observed from the TEM images. Based on the effects on peptide aggregation determined by ThT assay and TEM/AFM imaging, the inhibitory effects of the compounds follow the order $3 > 1 \approx 4 > 2$. Based on the molecular structure of the compounds, complex **2** contains a large aromatic ligand, whereas complex **3** is largely composed of an inorganic salt. This indicates that the inhibitory activity of each complex may utilize different molecular mechanisms.

ESI-MS analysis

ESI-MS was employed to analyze the mixture of peptides with the different vanadium complexes. Free PrP106-126 caused a peak at 1911.9 (1+), which corresponded to the expected mass (Fig. S7). Adding two equivalents of vanadium complexes caused the formation of various adducts (Fig. 5 & Table 2). Notably, these adducts contained a bi-oxygen species [PrP106-126+2O] for complexes **1**, **3**, and **4**, indicating possible oxidation. However, similar species were not present for complex **2** and the adduct was in the form of [PrP106-126+2VO+V(bipy)]. Mutant peptide M109F exhibited similar results, where a monooxygen species [M109F+1O] was obtained for complexes **1**, **3**, and **4**, whereas no adduct peaks were observed for complex **2** (Fig. S8). In order to identify the interactions of complex **2** with the peptide, ten equivalents of the complex were analyzed with the peptide. An adduct peak was identified as [M109F+V+VO+V(bipy)], suggesting binding of complex **2** with the peptide (Fig. S9). The differences between PrP106-126 and M109F could be attributed to the loss

of one methionine from the peptide sequence, which could be related to the methionine oxidation activity of the vanadium complexes.^{21,52,53}

NMR study

The histidine and two methionine residues in the peptide are critical factors for metal binding and peptide aggregation in PrP106-126.⁵⁴ The characteristic peaks for the His111 C δ Hs (7.09 ppm) and Met109/112 C ϵ Hs (2.08 ppm) were confirmed in the ¹H NMR spectrum of PrP106-126, as previously reported.^{6,54} After 3 h incubation of the vanadium complexes with the peptide, the His111 C δ Hs peak (7.09 ppm) shifted (Figs. 6 & S10–S12). Moreover, the 2.08 ppm peak disappeared and a new peak at 2.71 ppm emerged in the presence of complexes **1**, **3**, and **4**. Based on former results, the downfield shift of the 7.09 ppm peak could have been attributed to coordination of vanadium with the His111 side chain.^{55,56} Moreover, the methionine residues were oxidized as revealed by the MS spectra. For complex **2**, no change was found for the 2.08 ppm peak, indicating that the inhibitory activity of **2** with the peptide was different from the other 3 compounds. Similar results were obtained for the mutant peptide M109F (Figs. S13–S16). The 2.08 ppm peak can be assigned to the C ϵ Hs of Met112 and methionine oxidation of the peptide was observed with **1**, **3**, or **4**. Further NMR time-course experiments confirmed methionine oxidation (Fig. S17 & Table S1). The appearance of oxidized (2.71 ppm) and reduced states (2.08 ppm) indicated a slow-exchange over the course of the NMR experiment.⁵⁷ The oxidation process was characterized to occur via the interactions of methionine and H₂O₂ with vanadium

complexes.²¹ Through observation of the time-course experiments, the change in His111 C₃Hs was accomplished before the Met112 was completely oxidized, which implied that binding occurred prior to oxidation. In addition, oxidation of the peptide by the vanadium complex was faster than by H₂O₂ (Fig. S18 and Table S2).

K_d determination

Intrinsic fluorescence quenching was conducted to determine the binding affinity of metal complexes with the peptide, in which the phenylalanine residue in the peptide was excited and the dissociation constant (K_d) was estimated.⁴⁰ PrP106-126 contains no aromatic residues; thus, peptide M109F was used, and the fluorescence intensity at 287 nm of the M109F was measured in the presence of vanadium complex to calculate K_d through nonlinear least-squares regression.⁴⁸ The samples were prepared and assayed after a 3 h incubation to ensure to complete oxidation. The apparent K_d values were $5.4 \pm 0.1 \times 10^{-5}$, $5.1 \pm 0.4 \times 10^{-8}$, $1.5 \pm 0.1 \times 10^{-4}$, and $1.7 \pm 0.4 \times 10^{-6}$ M for complexes **1**, **2**, **3**, and **4**, respectively (Fig. 7). Complex **2** exhibited the strongest binding affinity and was an order of magnitude higher than the other three compounds. This observation suggests the occurrence of hydrophobic interactions between the complex with an aromatic ligand and the peptide M109F.¹³ However, **2** caused weaker inhibition, consistent with ThT assay and the TEM results.

HPLC analysis

HPLC was utilized to identify interactions of PrP106-126 with the vanadium complexes as HPLC can effectively separate amyloid proteins based on conformational changes.⁵⁸ PrP106-126 eluted from the column at 16.6 min and addition of the metal complexes reduced the elution time to 15.0, 14.9, and 16.0 min for complexes **1**, **3**, and **4**, respectively, whereas the elution time was extended to 18.1 min for complex **2** (Fig. 8). Similar results were obtained in M109F sample (Table 3). Changes in elution time revealed difference in peptide composition induced by interactions between the peptide and the vanadium complex. Together, the NMR and ESI-MS data suggested that the changes may have been due to methionine oxidation and direct binding between peptides and vanadium complexes.

Cell survival

Vanadium complexes caused a marked reduction in aggregation of prion peptides through direct binding and methionine oxidation. However, the ability of these complexes to decrease the neurotoxicity of PrP106-126 and its mutant peptide M109F still required investigation. Human SH-SY5Y neuroblastoma cells were used as controls and standardized to 100% viability. Cell survival was evaluated after treating the cells with either the peptide or a combination of peptide and vanadium complexes. Fig. 9 shows that PrP106-126 caused a decrease in cell viability to $36 \pm 0.3\%$ as determined by the MTT assay.⁴¹ Addition of complex **2** rescued the cell viability to $\sim 70\%$. Cell viability decreased as the concentration of complex **3** and **4** was increased, whereas cells viability was not affected by treatment with complex **1**. The cytotoxicity

of the mutant peptide M109F at $47\pm 0.2\%$ was less than PrP106-126. Cell viability was increased by addition of complexes **1**, **2**, and **3** (Fig. S19), however, complex **4** failed to increase cell viability of M109F-treated SH-SY5Y neuroblastoma cells. Vanadium complexes exhibited both toxic and beneficial effects on living systems.^{18,20} Although the vanadium complexes caused cytotoxicity in SH-SY5Y cells (Fig. S20), there was also a decrease in the neurotoxicity induced by PrP106-126 and M109F.

Discussion

Inhibition of peptide aggregation by vanadium complexes

Inhibition of amyloid fibril formation has led to the development and design of new medications against protein conformational diseases. Metal complexes are widely used as anticancer drugs and inhibitors which target specific proteins. Vanadium complexes have been utilized as insulin mimetic agents for >100 years.^{11,12} Previously, peroxovanadium complexes with aromatic ligands were found to inhibit the aggregation of $A\beta_{1-42}$ and PrP106-126.²¹ In the present study, different vanadium complexes were selected, ranging from a larger aromatic ligand (**2**) to a fully inorganic compound (**3**). The obtained results elucidated the role of ligand coordination and redox properties that arises from the vanadium compounds. Peptide aggregation analysis by ThT assay, TEM imaging, and AFM morphology elucidated that the four complexes inhibited fibril formation in PrP106-126 and peptide M109F. This inhibition was concentration-dependent and aggregation of peptide M109F was

weaker than PrP106-126. In addition, the roles of the four complexes were similar for both PrP106-126 and peptide M109F. Complex **3**, which lacked an aromatic ligand, exerted a notable inhibitory effect on peptide aggregation. The results suggest that methionine oxidation is crucial for inhibition of peptide aggregation. Compared to complexes **1**, **3**, and **4**, complex **2** had relatively weak inhibitory activity. As most amyloid peptides undergo conformational changes from β -sheets to oligomers/fibrils, compounds that bind to peptide do not cause conformational change, peptide aggregation is unlikely to be affected. Often, higher binding affinities do not result in higher levels of inhibition.

Mode of action of vanadium complexes with peptides

MS analysis indicated that incubating the peptide with complexes **1**, **3**, or **4** produced [PrP106-126+2O] and [M109F+1O] species for PrP106-126 and peptide M109F, respectively. These results indicate that oxidation of the peptide were due to reaction with the vanadium complex. Time-course NMR experiments were used to monitor the reaction, and methionine oxidation was observed. Moreover, NMR data identified that direct binding between peptide occurred prior to complete methionine oxidation, as indicated by shifts in the His111 side-chain peak. Interestingly, no oxygen adduct was noted by MS for the interaction of complex **2** with the peptide. Combining the data from MS and NMR analyses, as well as K_d determination, complex **2** might bind to the peptide by hydrophobic interactions and metal coordination. The results for complex **2** were distinct from the other three compounds, as demonstrated by NMR

and HPLC. Specific structural features of **2** contributed to its different inhibitory effects, as reflected by ThT assay and TEM/AFM images. Compared with bipyridine and phenanthroline ligands,²¹ the increased ligand steric effect in **2** inhibited the methionine oxidation activity of vanadate. Therefore, **2** had a different mechanism for inhibiting the aggregation of PrP106-126 and peptide M109F.

Peroxovanadium complexes also affect hIAPP fibrillization, principally through hydrophobic and electrostatic interactions.¹³ This difference largely results in discrepancies between various peptide sequences, given that methionine is absent in hIAPP. Methionine residue can be easily oxidized by oxodiperoxovanadate complexes and oxidation significantly affects the pathogenic aggregation of amyloid proteins, including A β , α -synuclein, and PrP.⁵⁹⁻⁶¹ This role may be attributed to the higher polarity and decreased flexibility of methionine sulfoxide in comparison to peptides that contain methionine residues.⁶²⁻⁶⁵ However, modification of ligand characteristics may change and eliminate oxidative activity, as indicated by results with **2**.

Neurotoxicity of prion peptides

The oxodiperoxovanadate complexes effectively influenced the neurotoxicity induced by both PrP106-126 and peptide M109F. Complexes **1** and **4** caused a decrease in the aggregation of PrP106-126, as observed by ThT assay and TEM/AFM images. However, the effect of these complexes on cytotoxicity was less than that of complex **2**. Although the inhibitory effects of **2** on peptide fibril formation were less

pronounced than other compounds, it had a greater effective on enhancing cell viability in the presence of prion peptides. The cytotoxicity induced by amyloid peptides predominantly results from the toxicity of oligomers and methionine oxidation could cause the peptide to remain in a monomeric state.⁵⁹ However, the efficacy of complex **2** could also be attributed to the decreased cytotoxicity of the compound itself. Different from the other complexes, complex **2** interacted with the peptides mainly via hydrophobic interactions.

Conclusion

This study investigated the mechanism of oxodiperoxovanadate complexes with amyloid peptides PrP106-126 and mutant peptide M109F. Together, the results indicated that oxodiperoxovanadate complexes significantly inhibited the formation of amyloid fibrils. The interaction of complexes **1**, **3**, and **4** with the peptides mainly resulted in methionine oxidation due to their distinct redox properties, which effectively inhibited peptide aggregation. Meanwhile, complex **2** interacted with the peptides mainly through hydrophobic interactions. The role of the aromatic ligand is significant, as it changed the mechanism of peptide binding due to steric effects. Although **3** exhibited improved inhibitory effects on peptide aggregation, complex **2** caused the most apparent reduction in cytotoxicity induced by peptide aggregation. The differences in inhibition between the complexes may depend on molecular redox properties and aromaticity of the ligand. This study provides valuable information on the treatment of amyloid fibrillization using vanadium complexes. However, the

structure–activity relationship between different complexes and amyloid peptides requires further investigation.

Acknowledgements

The work was supported by the National Natural Science Foundation of China (No. 21473251 and No. 21271185), the Fundamental Research Funds for the Central Universities, and the Research Fund of Renmin University of China (RUC No.15XNLQ04).

References

1. Y. Jung and S. J. Lippard, *Chem. Rev.*, 2007, **107**, 1387–1407.
2. K. Yan, C. N. Lok, K. Bierla and C. M. Che, *Chem. Commun.*, 2010, **46**, 7691–7693.
3. H. Chen, J. A. Parkinson, S. Parsons, R. A. Robert, R. O. Gould and P. J. Sadler, *J. Am. Chem. Soc.*, 2002, **124**, 3064–3082.
4. K. J. Barnham, V. B. Kenche, G. D. Ciccotosto, D. P. Smith, D. J. Tew, X. Liu, K. Perez, G. A. Cranston, T. J. Johanssen, I. Volitakis, A. I. Bush, C. L. Masters, A. R. White, J. P. Smith, R. A. Cherny and R. Cappai, *Proc. Natl. Acad. Sci. U.S.A.*, 2008, **105**, 6813–6818.
5. L. He, X. Wang, C. Zhao, H. Wang and W. Du, *Metallomics*, 2013, **5**, 1599–1603.
6. X. Wang, L. He, C. Zhao, W. Du and J. Lin, *J. Biol. Inorg. Chem.*, 2013, **18**, 767–778.
7. W. J. Geldenhuys and C. J. Van der Schyf, *Curr. Med. Chem.*, 2013, **20**, 1662–1672.
8. D. J. Hayne, S. Li and P. S. Donnelly, *Chem. Soc. Rev.*, 2014, **43**, 6701–6715.
9. G. Grasso and S. Bonnet, *Metallomics*, 2014, **6**, 1346–1357.
10. H. Sakurai, *Chem. Rec.*, 2002, **2**, 237–248.
11. K. H. Thompson, J. Lichter, C. LeBel, M. C. Scaife, J. H. McNeill and C. Orvig, *J. Inorg. Biochem.*, 2009, **103**, 554–558.
12. K. H. Thompson, J. H. McNeill and C. Orvig, *Chem. Rev.*, 1999, **99**, 2561–2571.
13. L. He, X. Wang, C. Zhao, D. Zhu and W. Du, *Metallomics*, 2014, **6**, 1087–1096.
14. V. G. Yuen, C. Orvig and J. H. McNeill, *Can. J. Physiol. Pharmacol.*, 1993, **71**, 263–269.
15. V. G. Yuen, P. Caravan, L. Gelmini, N. Glover, J. H. McNeill, I. A. Setyawati, Y. Zhou and C. Orvig, *J. Inorg. Biochem.*, 1997, **68**, 109–116.
16. J. Benítez, L. Becco, I. Correia, S. M. Leal, H. Guiset, J. C. Pessoa, J. Lorenzo, S. Tanco, P. Escobar and V. Moreno, *J. Inorg. Biochem.*, 2011, **105**, 303–312.
17. T. L. Turner, V. H. Nguyen, C. C. McLauchlan, Z. Dymon, B. M. Dorsey, J. D. Hooker and M.

- A. Jones, *J. Inorg. Biochem.*, 2012, **108**, 96–104.
18. O. J. D’Cruz, Y. Dong and F. M. Uckun, *Biochem. Biophys. Res. Commun.*, 2003, **302**, 253–264.
19. J. H. Hwang, R. K. Larson and M. M. Abu-Omar, *Inorg. Chem.*, 2003, **42**, 7967–7977.
20. J. Benítez, L. Guggeri, I. Tomaz, G. Arrambide, M. Navarro, J. C. Pessoa, B. Garat and D. Gambino, *J. Inorg. Biochem.*, 2009, **103**, 609–616.
21. L. He, X. Wang, C. Zhao, D. Zhu and W. Du, *Metallomics*, 2015, **7**, 1562–1572.
22. J. Collinge, *J. Neurol. Neurosurg. Psychiatry*, 2005, **76**, 906–919.
23. A. Maheshwari, M. Fischer, P. Gambetti, A. Parker, A. Ram, C. Soto, L. C. Marambio, Y. Cohen, E. D. Belay, R. A. Maddox, S. Mead, C. Goodman, J. S. Kass, L. B. Schonberger and H. M. Hussein, *Emerg. Infect. Dis.*, 2015, **21**, 750-759.
24. W. J. Huang, W. W. Chen, X. Zhang, *Eur. Rev. Med. Pharmacol.*, 2015, **19**, 4028-4034.
25. E. A. Asante, M. Smidak, A. Grimshaw, R. Houghton, A. Tomlinson, A. Jeelani, T. Jakubcova, S. Hamdan, A. Richard-Londt, J. M. Linehan, S. Brandner, M. Alpers, J. Whitfield, S. Mead, J. D. F. Wadsworth and J. Collinge, *Nature*, 2015, **522**, 478-481.
26. C. Korth, B. Stierli, P. Streit, M. Moser, O. Schaller, R. Fischer, W. Schulz-Schaeffer, H. Kretzschmar, A. Raeber, U. Braun, F. Ehrensperger, S. Hornemann, R. Glockshuber, R. Riek, M. Billeter, K. Wuthrich and B. Oesch, *Nature*, 1997, **390**, 74–77.
27. S. B. Prusiner, *Science*, 1997, **278**, 245–251.
28. G. Forloni, N. Angeretti, R. Chiesa, E. Monzani, M. Salmona, O. Bugiani and F. Tagliavini, *Nature*, 1993, **362**, 543–546.
29. S. B. Prusiner, *Proc. Natl. Acad. Sci. U. S. A.*, 1998, **95**, 13363–13383.
30. P. Walsh, K. Simonetti and S. Sharpe, *Structure*, 2009, **17**, 417–426.
31. M. Salmona, P. Malesani, L. De Gioia, S. Gorla, M. Bruschi, A. Molinari, F. Della Vedova, B. Pedrotti, M. Marrari and T. Awan, *Biochem. J.*, 1999, **342**, 207–214.
32. S. Vilches, C. Vergara, O. Nicolás, G. Sanclimens, S. Merino, S. Varón, G. A. Acosta, F. Albericio, M. Royo and J. A. DelRío, *PLoS One*, 2013, **8**, e70881.
33. C. N. O’Donovan, D. Tobin and T. G. Cotter, *J. Biol. Chem.*, 2001, **276**, 43516–43523.
34. T. Florio, M. Grimaldi, A. Scorziello, M. Salmona, O. Bugiani, F. Tagliavini, G. Forloni and G. Schettini, *Biochem. Biophys. Res. Commun.*, 1996, **228**, 397–405.
35. T. Florio, S. Thellung, C. Amico, M. Robello, M. Salmona, O. Bugiani, F. Tagliavini, G. Forloni and G. Schettini, *J. Neurosci. Res.*, 1998, **54**, 341–352.
36. L. Vella, A. F. Hill and R. Cappai, *Neurodegeneration and Prion Disease*. Springer, 2005, 217–240.
37. Y. Porat, A. Abramowitz and E. Gazit, *Chem. Biol. Drug Des.*, 2006, **67**, 27–37.
38. M. Tatarek-Nossol, L. M. Yan, A. Schmauder, K. Tenidis, G. Westermark and A. Kapurniotu, *Chem. Biol.*, 2005, **12**, 797–809.
39. X. Wang, L. He, C. Zhao, Y. Wang, L. Hei, M. Cui, X. Zhu and W. Du, *J. Biol. Inorg. Chem.*, 2013, **128**, 1-10.
40. C. Zhao, X. Wang, L. He, B. Wang and W. Du, *Metallomics*, 2014, **6**, 2117-2125.
41. X. Wang, D. Zhu, C. Zhao, L. He and W. Du, *Metallomics*, 2015, **7**, 837-846.
42. X. Wang, M. Cui, C. Zhao, L. He, D. Zhu, B. Wang and W. Du, *Inorg. Chem.*, 2014, **53**, 5044-5054.
43. Ing-Britt Svensson and R. Stomberg, *Acta Chem. Scand.*, 1971, **25**, 898-910.

44. N. Vuletić and C. Djordjević, *J. Chem. Soc., Dalton Trans.*, 1973, 1137–1141.
45. H. Szentivanyi and R. Stomberg, *Acta Chem. Scand. A.*, 1984, **38**, 101–107.
46. M. K. Chaudhuri and N. S. Islam, *Transit. Metal. Chem.*, 1985, **10**, 333–335.
47. C. Djordjevic, B. C. Puryear, N. Vuletic, C. J. Abelt and S. J. Sheffield, *Inorg. Chem.*, 1988, **27**, 2926–2932.
48. D. Jiang, X. Li, R. Williams, S. Patel, L. Men, Y. Wang and F. Zhou, *Biochemistry*, 2009, **48**, 7939–7947.
49. L. Ronga, E. Langella, P. Palladino, D. Marasco, B. Tizzano, M. Saviano, C. Pedone, R. Improta and M. Ruvo, *Proteins*, 2007, **66**, 707–715.
50. J. H. Byun, H. Y. Kima, Y. S. Kima, I. M. Jung, D. J. Kim, W. K. Lee and K. H. Yoo, *Bioorg. Med. Chem. Lett.*, 2008, **18**, 5591–5593.
51. V. P. S. Chauhan, I. Ray, A. Chauhan, J. Wegiel and H. M. Wisniewski, *Neurol. Res.*, 1997, **7**, 805–809.
52. K. J. Binger, M. D. W. Griffin and G. J. Howlett, *Biochemistry*, 2008, **47**, 10208–10217.
53. S. Nishino and Y. Nishida, *Inorg. Chem. Commun.*, 2001, **4**, 86–89.
54. E. Gaggelli, F. Bernardi, E. Molteni, R. Pogni, D. Valensin, G. Valensin, M. Remelli, M. Luczkowski and H. Kozlowski, *J. Am. Chem. Soc.*, 2005, **127**, 996–1006.
55. Y. Wang, J. Xu, L. Wang, B. Zhang and W. Du, *Chem. Eur. J.*, 2010, **16**, 13339–13342.
56. Y. Wang, L. Feng, B. Zhang, X. Wang, C. Huang, Y. Li and W. Du, *Inorg. Chem.*, 2011, **50**, 4340–4348.
57. M. P. Williamson, *Prog. Nucl. Magn. Reson. Spectrosc.*, 2013, **73**, 1–16.
58. J. R. Requena, M. N. Dimitrova, G. Legnameb, S. Teijeirae, S. B. Prusiner and R. L. Levinea, *Arch. Biochem. Biophys.*, 2004, **432**, 188–195.
59. M. Grabenauer, C. Wu, P. Soto, J. E. Shea and M. T. Bowers, *J. Am. Chem. Soc.*, 2010, **132**, 532–539.
60. V. N. Uversky, G. Yamin, P. O. Souillac, J. Goers, C. B. Glaser and A. L. Fink, *FEBS Lett.*, 2002, **517**, 239–244.
61. W. Vogt, *Free Radical Biol. Med.*, 1995, **18**, 93–105.
62. L. Breydo, O. V. Bocharova, N. Makarava, V. V. Salnikov, M. Anderson and I. V. Baskakov, *Biochemistry*, 2005, **44**, 15534–15543.
63. M. J. Davies, *Biochim. Biophys. Acta, Proteins Proteomics*, 2005, **1703**, 93–109.
64. M. C. Miotto, E. E. Rodriguez, A. A. Valiente-Gabioud, V. Torres-Monserrat, A. S. Binolfi, L. Quintanar, M. Zweckstetter, C. Griesinger and C. O. Fernández, *Inorg. Chem.*, 2014, **53**, 4350–4358.
65. S. D. Maleknia, N. Reixach and J. N. Buxbaum, *FEBS J.*, 2006, **273**, 5400–5406.

Table 1 IC₅₀ values for different complex with the two peptides.

Vanadium complexes	IC ₅₀ values ^a (μM)	
	PrP106-126, A	M109F, B
[NH ₄] ₃ [VO(O ₂) ₂ (ox)]·2H ₂ O	28.10±0.60	21.50±1.5
(H ₂ bipy)[V ₂ O ₂ (O ₂) ₄ (bipy) ₂]·6H ₂ O	77.50±2.50	89.75±0.26
Na[VO(O ₂) ₂]·Na ₂ SO ₄	14.88±0.13	10.65±1.35
K ₂ [nicH{VO(O ₂) ₂ } ₂]·H ₂ O	16.55±0.45	16.89±0.94

^a Values were measured by the ThT fluorescence.

Table 2 The adduct peak analysis of ESI-MS spectra at two equivalents of oxodi-peroxovanadate complexes.

Complex	PrP106-126			M109F		
	Calcd	Measd	Binding species	Calcd	Measd	Binding species
1	1928.0(1+)	1929.4(1+)	PrP106-126+1O	1944.0(1+)	1946.0(1+)	M109F+1O
	1944.0(1+)	1947.0(1+)	PrP106-126+2O	3888.0(1+)	3889.0(1+)	2M109F+2O
	2291.9(1+)	2290.3(1+)	PrP106-126+VO+2V(ox)+2O			
2	1912.0(1+)	1915.0(1+)	PrP106-126	642.7(3+)	643.3(3+)	M109F
	2253.2(1+)	2257.0(1+)	PrP106-126+2VO+V(bipy)	964.0(4+)	965.0(4+)	2M109F
3	1928.0(1+)	1931.0(1+)	PrP106-126+1O	1928.0(1+)	1928.0(+)	M109F
	2272.9(1+)	2273.0(1+)	PrP106-126+3VO ₃ +4O	1944.0(1+)	1944.5(1+)	M109F+1O
4	1928.0(1+)	1931.0(1+)	PrP106-126+1O	648.0(3+)	648.7(3+)	M109F+1O
	1944.0(1+)	1947.0(1+)	PrP106-126+2O	972.0(2+)	973.0(2+)	M109F+1O
	2026.9(1+)	2027.0(1+)	PrP106-126+VO ₄			
	2292.2(1+)	2290.4(1+)	PrP106-126+2VO(nic)			

Table 3 The retention time of HPLC for two peptides in the presence of two equivalents of diverse vanadium complexes.

System	Time/min	System	Time/min
PrP106-126	16.58	M109F	17.96
PrP106-126+1	14.96	M109F+1	16.44
PrP106-126+2	16.63, 18.07	M109F+2	17.65, 19.11
PrP106-126+3	14.98	M109F+3	16.41
PrP106-126+4	15.95	M109F+4	16.72

Figure Captions

Scheme 1 The molecular structures of vanadium compounds. Complex **2** is presented in its 5H₂O form.

Fig. 1 ThT assay for the peptide aggregation in the absence (black) and presence of two equivalents of **1** (red), **2** (blue), **3** (magenta) and **4** (olive). (A) PrP106-126, (B) peptide M109F. ThT (navy) was used as a marker. The concentration of peptide was 100 μ M.

Fig. 2 TEM images of PrP106-126 in the absence (A) and presence of two equivalents of **1** (B), **2** (C), **3** (D) and **4** (E) . The scale bar is 100 nm.

Fig. 3 TEM images of PrP106-126 in the absence (A) and presence of ten equivalents of **1** (B), **2** (C), **3** (D) and **4** (E) . The scale bar is 500 nm.

Fig. 4 AFM images of peptide PrP106-126 in the absence (A) and presence of two equivalents of **1** (B), **2** (C), **3** (D) and **4** (E). The scale bar is 1 μ m.

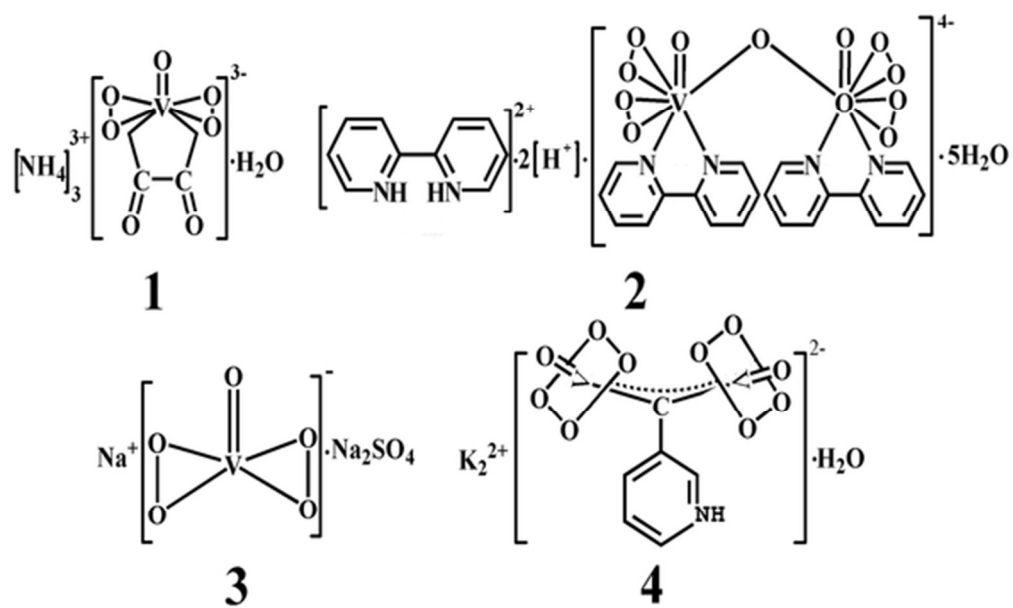
Fig. 5 ESI-MS spectra for the peptide PrP106-126 in the presence of two equivalents of **1** (A), **2** (B), **3** (C) and **4** (D).

Fig. 6 ¹H NMR spectra of PrP106-126 in the presence (A) and absence (B) of **1**. The marked peaks at 7.09 ppm and 2.08 ppm are ascribed to the side chain of His111 and Met109/112. The peak at 2.71 ppm is attributed to methyl protons of oxidized methionines. Addition of **1** made the peak at 7.09 ppm shift toward down-field.

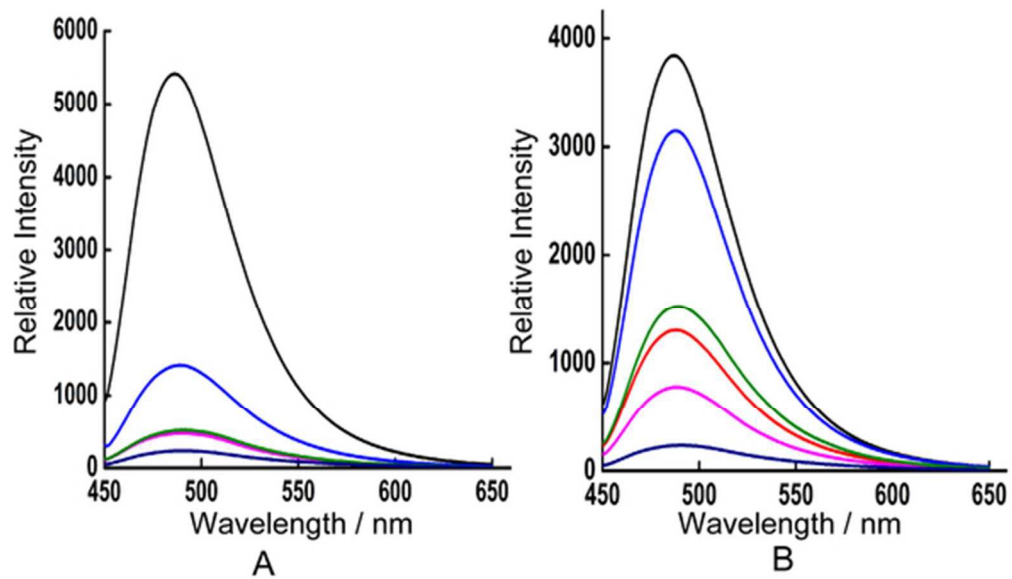
Fig. 7 *K_d* determination by fluorescence quenching method using the peptide M109F in the presence of **1** (A), **2** (B), **3** (C) and **4** (D).

Fig. 8 HPLC analysis for PrP106-126 (A) and peptide M109F (B) in the absence (a) and presence of **1** (b), **2** (c), **3** (d) and **4** (e). The concentration of PrP106-126 and M109F used was 50 mM and the vanadium complex used was 100 mM. The determination was performed after 24 h incubation.

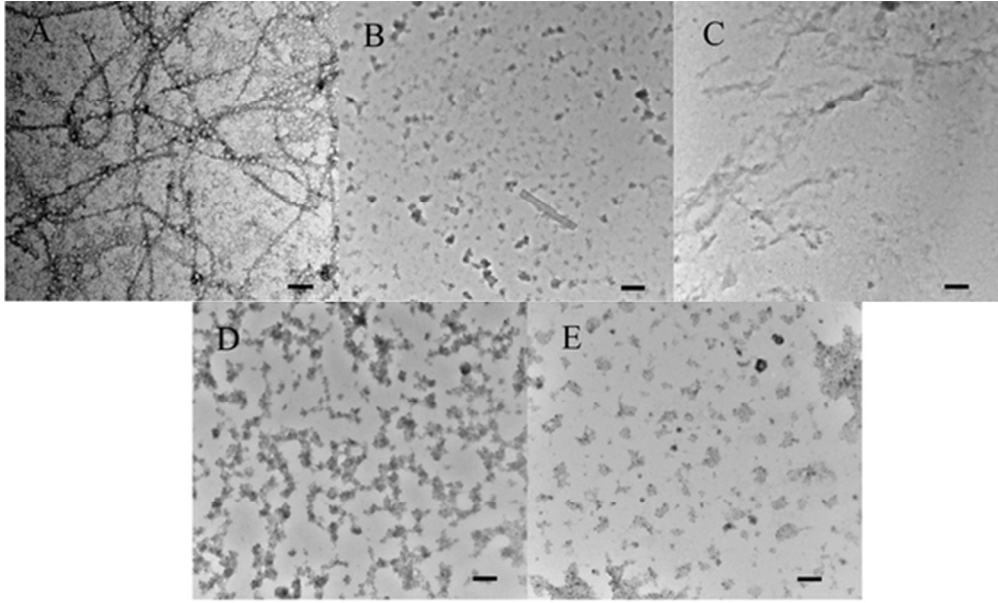
Fig. 9 Cell viability was monitored using the MTT assay. SH-SY5Y cells were treated with peptide PrP106-126 and different concentrations of vanadium complexes, i.e. 1.0 μ M (olive), 10 μ M (red) and 50 μ M (blue). The cytotoxicity test of PrP106-126 alone (olive) was used for comparison. The data are shown as means \pm SD n=3.** p<0.01 and *p<0.05 compared to the control.



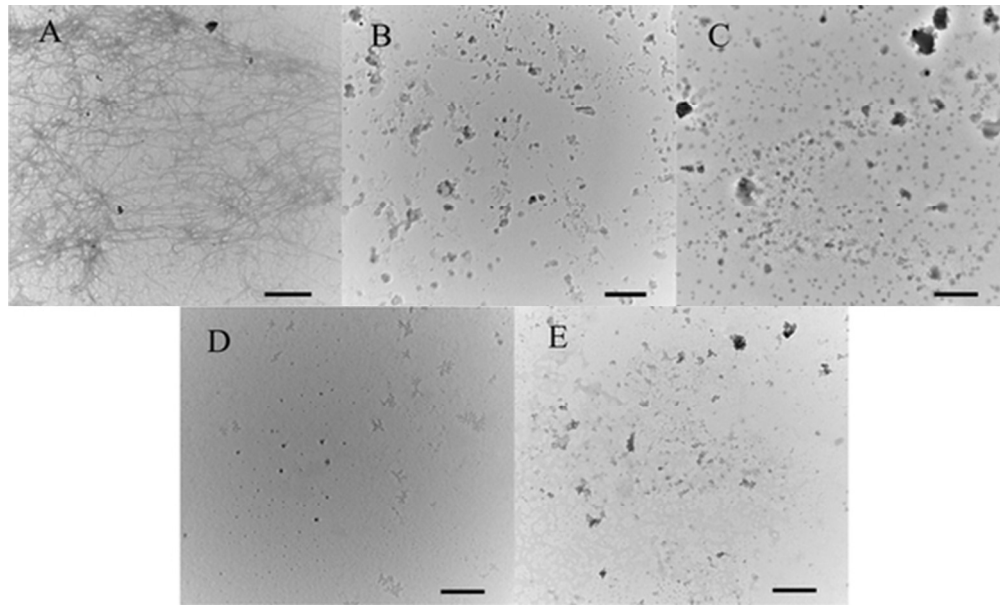
49x30mm (300 x 300 DPI)



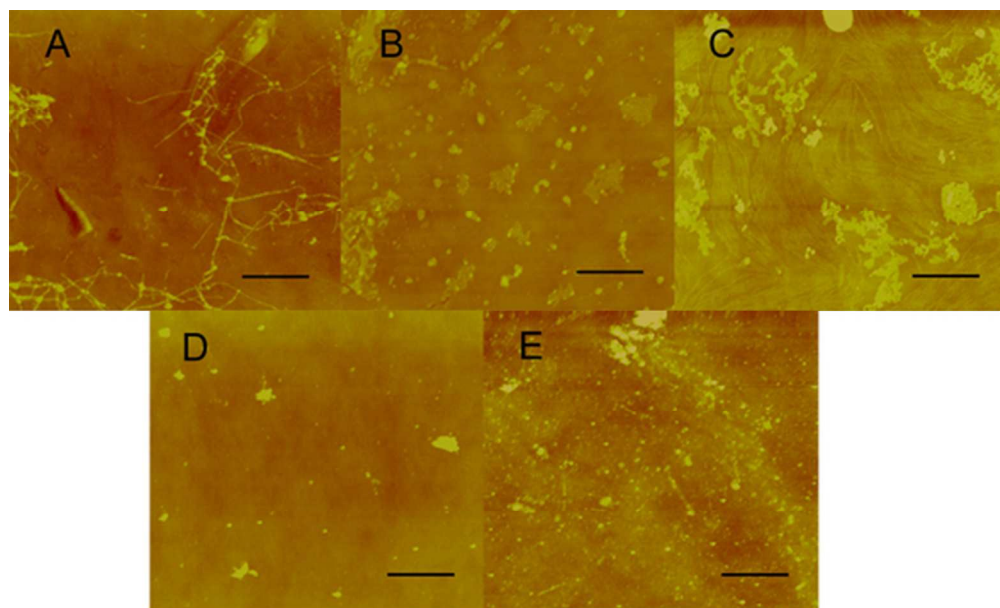
49x30mm (300 x 300 DPI)



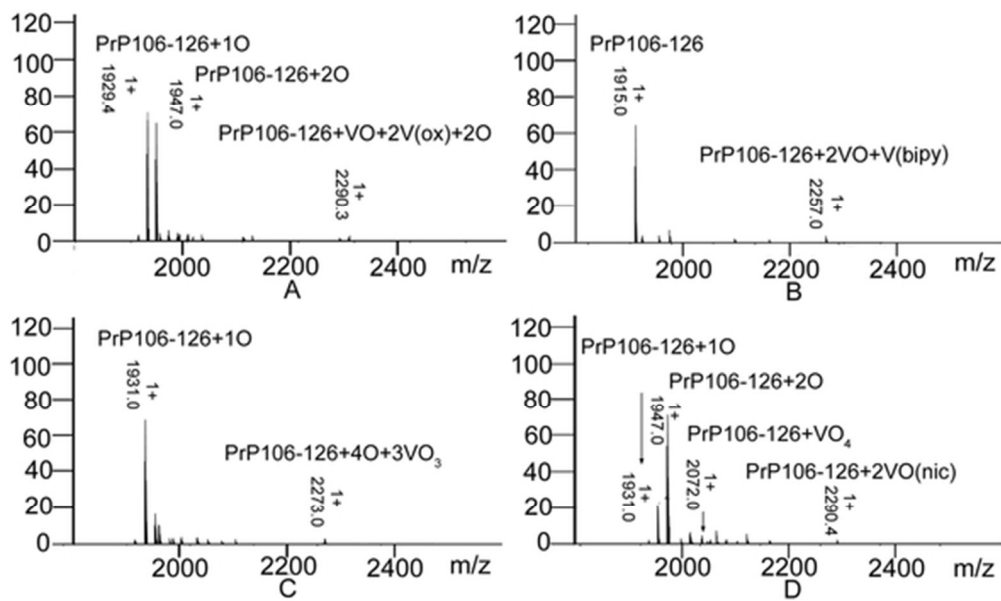
49x30mm (300 x 300 DPI)



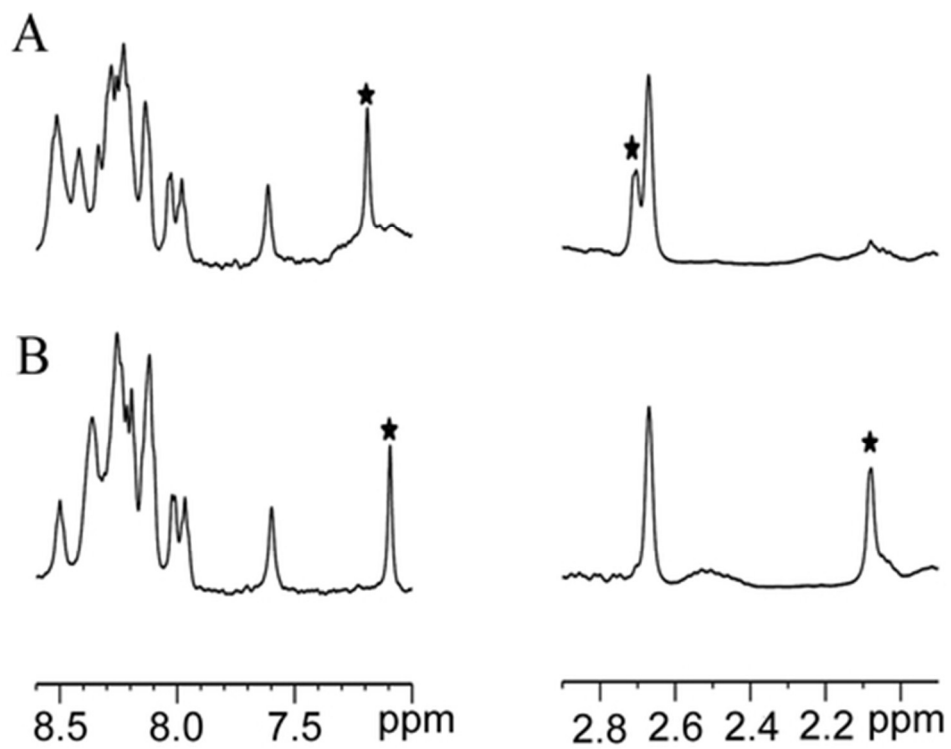
49x30mm (300 x 300 DPI)



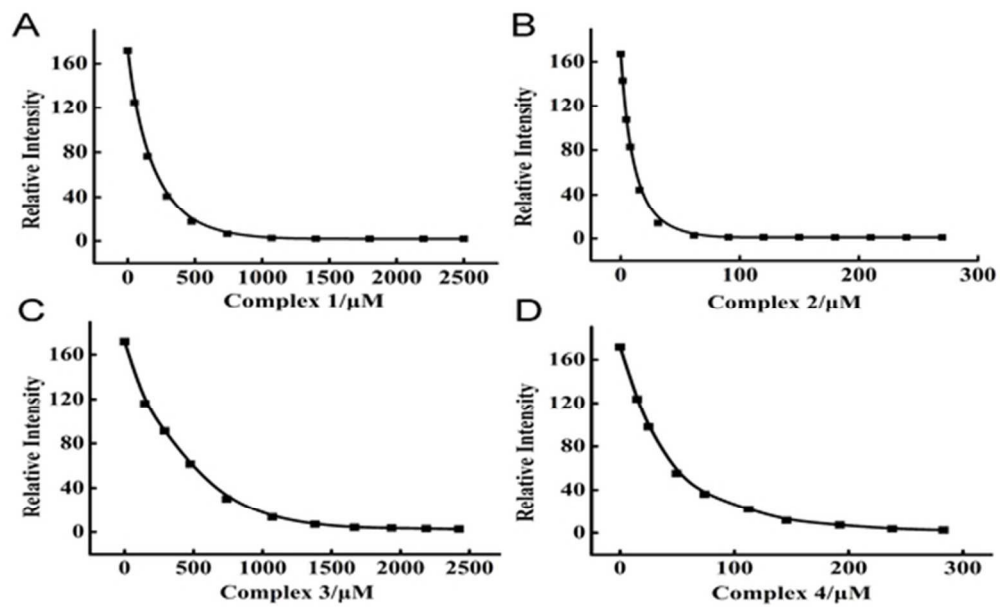
49x30mm (300 x 300 DPI)



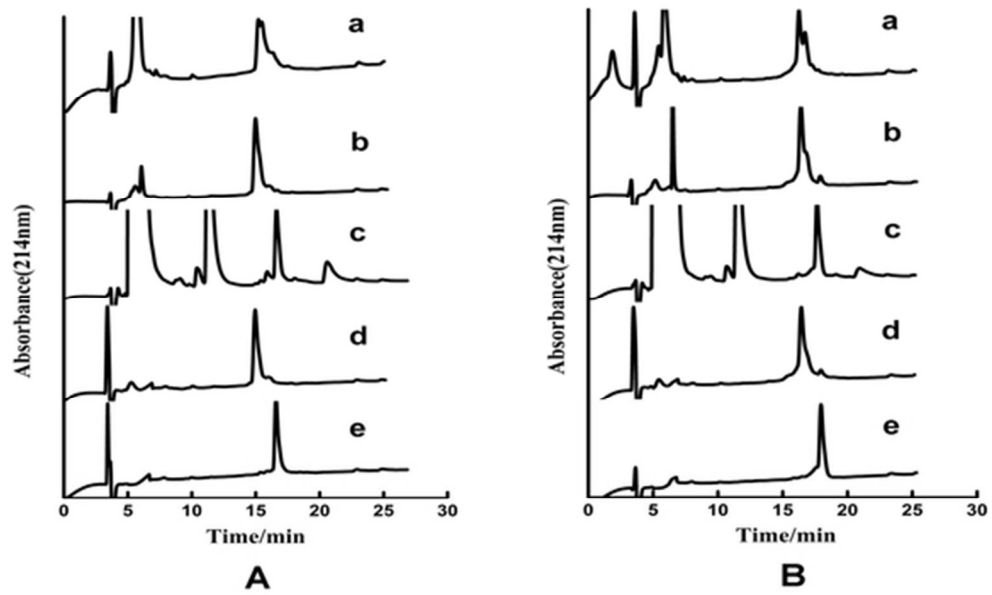
49x30mm (300 x 300 DPI)



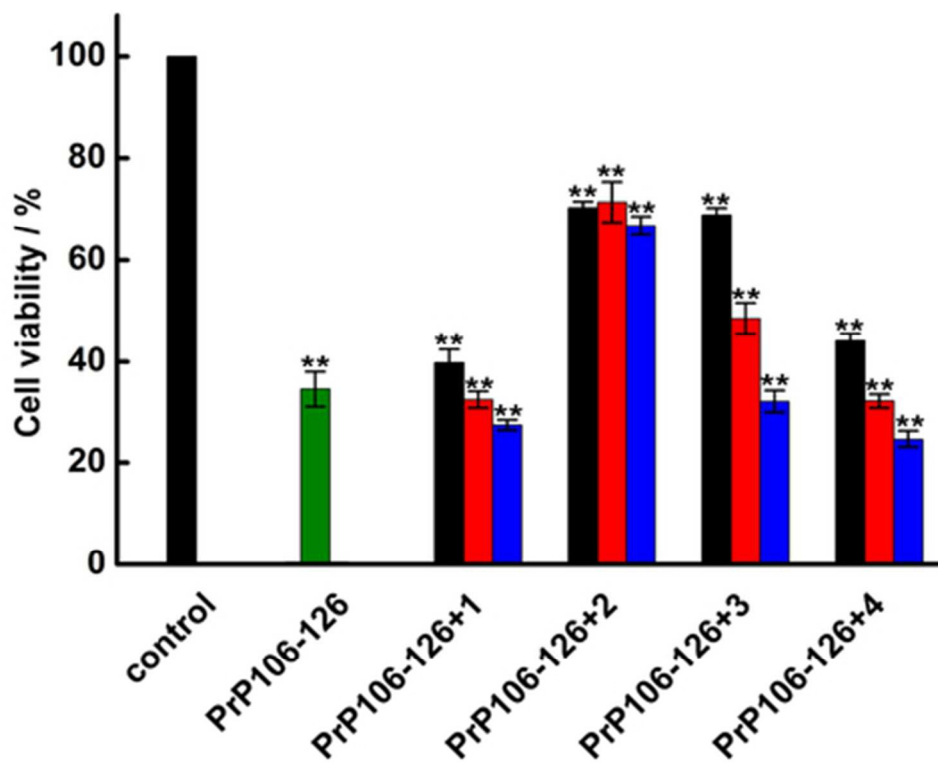
39x32mm (300 x 300 DPI)



49x30mm (300 x 300 DPI)

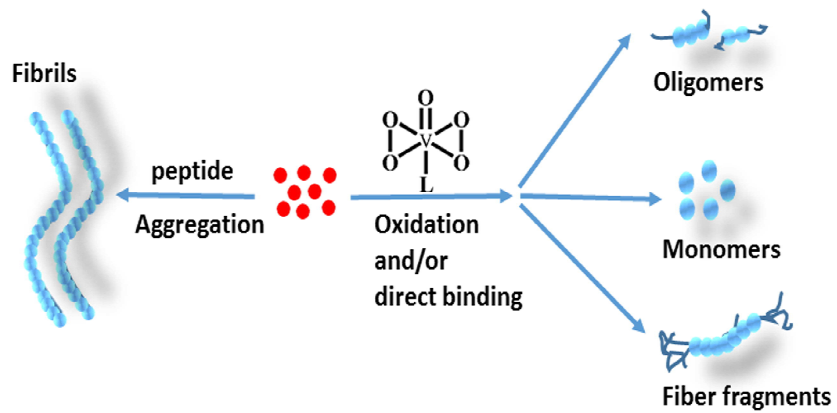


49x30mm (300 x 300 DPI)



39x32mm (300 x 300 DPI)

Graphic Abstract



Different oxodiperoxovanadate complexes inhibit the fibril formation of prion neuropeptides by different action mode.